HHS Public Access

Author manuscript

J Phys Chem B. Author manuscript; available in PMC 2019 August 19.

Published in final edited form as:

J Phys Chem B. 2018 December 13; 122(49): 11792–11799. doi:10.1021/acs.jpcb.8b08456.

Interrupted Pressure-Jump NMR Experiments Reveal Resonances of On-Pathway Protein Folding Intermediate

Cyril Charlier[‡], **Joseph M. Courtney**[‡], **Philip Anfinrud**, **Ad Bax**

Laboratory of Chemical Physics, NIDDK, National Institutes of Health, Bethesda, MD, 20892-0520, USA

Abstract

Previous pressure-jump NMR experiments on a pressure-sensitized double mutant of ubiquitin showed evidence that its folding occurs via two parallel, comparably efficient pathways: A single barrier and a two-barrier pathway. An interrupted folding NMR experiment is introduced, where for a brief period the pressure is dropped to atmospheric conditions (1 bar), followed by a jump back to high pressure for signal detection. Conventional, forward sampling of the indirect dimension during the low-pressure period correlates the ^{15}N or ^{13}C′ chemical shifts of the unfolded protein at 1 bar to the ^{1}H frequencies of both the unfolded and folded proteins at high pressure. Remarkably, sampling the data of the same experiment in the reverse direction yields the frequencies of proteins present at the end of the low-pressure interval, which include unfolded, intermediate, and folded species. Although the folding intermediate ^{15}N shifts differ strongly from natively folded protein, its ^{13}C′ chemical shifts, which are more sensitive probes for secondary structure, closely match those of the folded protein and indicate that the folding intermediate must have a structure that is quite similar to the native state.

Keywords

protein folding; pressure jump; folding pathway; folding intermediate; chemical shift; NMR; ubiquitin

INTRODUCTION

Proteins transition from their initially highly disordered to their well-defined native state on a time scale that is many orders of magnitude faster than would be expected from a random search of conformational space, pointing to the existence of pathways in this process.[1] For many small proteins, a single barrier on such pathways, separating the unfolded from the folded state, suffices to explain a large variety of experimental data, mostly derived from rapid mixing, stopped-flow experiments. It is now well established that the actual barrier crossing event is exceedingly fast and diffusion-limited,[2–5] and therefore difficult to observe directly. The presence of additional, lower barriers would result in short-lived intermediates,

Corresponding Author bax@nih.gov.

‡These authors contributed equally

Author Contributions

The manuscript was written through contributions of all authors. All authors have given approval to the final version of the manuscript.

which would have low populations and be difficult to detect. NMR relaxation dispersion measurements, which are exquisitely sensitive for identifying such lowly populated states, have characterized a highly transient, on-pathway folding intermediate for a Fyn-SH3 mutant,[6–8] suggesting that, perhaps, such intermediates are more prevalent than generally assumed. Most commonly, the protein folding process is probed by Trp fluorescence, fluorescence resonance energy transfer (FRET), or backbone amide hydrogen exchange.[9–13] NMR spectroscopy has played an important role in these latter studies, yielding highly quantitative site-specific hydrogen exchange rates with a temporal resolution that is only limited by the speed at which the exchange process can be quenched.[14–16] Such data yield the rates at which H-bonds form after initiation of the folding process. If differences in the hydrogen exchange protection profiles are seen for various regions of the protein, these data point to the presence of folding intermediates, i.e. multiple barriers on the folding pathway.[17–19] In such work, NMR spectroscopy is used in an indirect manner, to probe the exchange-quenched sample at residue-specific resolution, and comparable results now also have become accessible by advances in mass spectrometry, thereby requiring much less sample.[16, 20–21]

Direct monitoring of protein folding by NMR is also possible, but due to the long time required to generate an NMR spectrum such studies initially were limited to slower folding or unfolding systems.[22–25] However, improvements in technology about a decade ago have much increased the accessible time resolution.[26–27]

In non-equilibrium folding experiments, experimental conditions are typically changed abruptly from those favoring the unfolded state to those favoring the native state. This may be accomplished by a sudden jump in pH, dilution of denaturant, release of a co-factor, or by a sudden drop in hydrostatic pressure. The latter method, switching the pressure, is particularly benign, allowing the protein to be probed under native buffer conditions. However, a prerequisite for pressure-induced unfolding is that the protein volume of the unfolded state is substantially lower than that of the folded state, in practice by at least ~50 mL/mole. Equilibrium NMR spectra, recorded as a function of pressure, typically over the 0.1–3 kbar range, then often permit the simultaneous observation of unfolded and folded protein resonances in a slow exchange equilibrium, and can yield site-specific information on the state of each residue.[28–32] Analogous to pressure-jump fluorescence experiments,[33] the temporal change in the NMR spectrum following a step change in pressure can reveal kinetic information, provided the kinetics are slower than the duration of the pressure change, which often represents a challenging requirement for NMR spectroscopy.[25, 34] Recently, this limitation has been addressed by the development of dedicated hardware that rapidly increases or decreases the pressure in the NMR sample cell in a manner synchronized with the data acquisition process.[35–36] The ability to repeat the pressure-jump process thousands of times then provides access to processes on time scales much faster than those needed to collect an entire multi-dimensional NMR spectrum.[26, 36–37]

In our first application of the newly developed pressure jump NMR hardware, we studied ubiquitin, sensitized to pressure by the introduction of two Val to Ala cavity-generating mutations (V17A and V26A), while retaining the same native structure as the wild-type protein.[36, 38] Below, this double mutant is referred to as VA2-ubiquitin. Ubiquitin has

functioned as a model protein in numerous experimental and computational folding studies,[27, 39–49] and is very well suited for detailed NMR studies, therefore providing a perfect system for technological and methodological developments. Prior work citing evidence for an intermediate in ubiquitin's folding pathway,[13, 39, 50] has been contested.[51] Our work conclusively showed the presence of parallel, single-barrier and double-barrier pathways, with their relative efficiency being a strong function of temperature.[36] A separate $C^{\delta 2}H_3$ signal for Leu-50 was transiently visible for the double barrier intermediate,[36] and the average ^{15}N chemical shift during the folding process deviated from two-state behavior. This latter observation enabled estimation of the folding intermediate chemical shifts, which differed very substantially from those of both the unfolded and folded native states of the protein.[52] Remarkably, the hydrogen exchange protection of the intermediate and folded states were found to be very similar, with significantly lower protection only observed for two residues in the folding intermediate.[38]

Here, we demonstrate that direct observation of the ^{15}N and $^{13}C'$ chemical shifts of the folding intermediate becomes accessible by very minor modifications of a commonly used pulse scheme, where signals are digitized in a direction opposite to that conventionally used. For samples at equilibrium, the direction of sampling has no impact on the spectrum. In contrast, for the non-equilibrium, folding experiments, the forward and reverse sampled spectra are quite different. Significantly, reverse sampled spectra yield chemical shifts of the folding intermediate that are the first step towards determining its detailed molecular structure.

RESULTS AND DISCUSSION

Forward sampled pressure-jump HSQC and HNCO pulse schemes.

The NMR resonance frequencies of both the folded and unfolded states of a protein are quite sensitive to hydrostatic pressure.[30, 53] Switching of the pressure during an NMR pulse scheme therefore is preferably performed during a period where the magnetization is stored along the z axis, such that small fluctuations in the timing of the switching that are invariably associated with the mechanical movement of the valve have minimal effect on the observed signal. Many NMR pulse sequences have such periods built into them naturally, and often utilize such delays to apply pulsed field gradients to remove spurious magnetization transfer pathways.[54–55] For example, in the in-phase, composite-pulse-decoupled heteronuclear single quantum correlation (HSQC) experiment,[56] the intervals just after the first refocused INEPT transfer of $^1H^N$ magnetization to ^{15}N, and prior to reverse INEPT transfer back to $^1H^N$, can be used for this purpose (SI Figure 1A). A fully analogous scheme, which is essentially a two-dimensional version of the common HNCO experiment,[57] can be used to transfer magnetization from H_z to C'_zN_z, prior to generating transverse $^{13}C'$ magnetization by a 90° $^{13}C'$ pulse (SI Figure 1C). In our pressure-jump experiments, the pressure is dropped to 1 bar just after completing the first magnetization transfer from ^1H to ^{15}N (for HSQC), or to C'_zN_z (for HNCO; Figure 1). We allow the folding to occur for a low-pressure duration T, during which ^{15}N or $^{13}C'$ chemical shift is encoded for a variable t_1 evolution period. When recorded in the usual, forward manner (Figure 1B, Top), the

signal intensity at the end of the low-pressure period, prior to reverse INEPT transfer to ^{1}H, is proportional to

$$M_z(t_1) = [U]_0 \cos\left(\omega_x t_1\right) \exp\left(-R_2^U \; t_1\right) \quad 1$$

where ω_X denotes the angular ^{15}N or $^{13}C'$ frequency of the unfolded protein, assuming no residual folded protein remains present at the end of the high-pressure preparation period. $[U]_0$ is the concentration of unfolded protein present at the start of the low-pressure period. R_2^U corresponds to the sum of the transverse relaxation rate of the unfolded species, R_2, and the forward folding rates, $k_{U\rightarrow I}$ and $k_{U\rightarrow F}$, from the unfolded to the intermediate (two-barrier pathway) and from the unfolded to the folded state (single-barrier pathway), respectively.

Concentrations of the three species (plotted in Figure S2A), unfolded [U(t)], intermediate [I(t)], and folded [F(t)], at time t after the pressure drop are given by:

$$[U](t) = [U]_0 exp(-k't) \quad 2a$$

$$[I](t) = [U]_0\left(\frac{k_{U\rightarrow I}}{-k' + k_{I\rightarrow F}}\right)\left[exp(-k't) - exp\left(-k_{I\rightarrow F}t\right)\right] \quad 2b$$

$$[F](t) = [U]_0 - [U](t) - [I](t) \quad 2c$$

With $k' = \; k_{U\rightarrow I} + k_{U\rightarrow F}$.

While a fraction of protein will fold after the switch to low pressure and will precess with a folded chemical shift for the remainder of the t_1 period, its signal will remain invisible in the HSQC spectrum as any signal with zero intensity t_1=0 will have an integral of zero in the resulting spectrum. Moreover, the transverse phase of magnetization of a protein that switches from unfolded to folded at time τ after the first 90° pulse accumulates a transverse phase $\omega_U\tau$ and will evolve for the remainder of t_1 with ω_F. At the end of the t_1 evolution period its phase will be $\omega_U\tau + \omega_F(t_1 - \tau)$ and signals from proteins that switched to the folded state at different values of τ therefore will destructively interfere with one another (unless $\omega_U \approx \omega_F$) and not contribute significantly to observed signal (Figure S2A, S3). The same applies for any folding intermediate signal. Note that weak signals of the intermediate state are visible in the noise-free simulations (Figure S3B,D), but result from proteins that refolded during the "padding delay" between the pressure drop and the actual start of t_1 evolution (*ca.* 5 ms), included in the simulations, but below the detection threshold in the experimental spectra. The final, forward-sampled spectrum therefore yields resonances that carry the unfolded ^{15}N frequency at 1 bar in the F_1 dimension of the final 2D spectrum,

correlated to $^{1}H^{N}$ frequencies of both the unfolded and folded protein at high-pressure in the F_2 dimension (Figure 2A and Figure S3B,D). Similarly, the forward sampled 2D HNCO spectrum shows $^{13}C'$ resonances of the unfolded protein at 1 bar (F_1 dimension) correlated to $^{1}H^{N}$ frequencies of the next residue for both the unfolded and folded protein at high pressure (Figure 3A). Note that the VA2-ubiquitin unfolding rate at room temperature is slow, and proteins that switch to the folded state during the low-pressure period have insufficient time to unfold prior to ^{1}H detection at high pressure (Figure S2A).

Reverse sampled, interrupted folding HSQC and HNCO pulse schemes.

Simply by changing the timing of the pulses that generate the t_1 modulation, the same pulse schemes used above for detection of the unfolded ^{15}N and $^{13}C'$ resonances at 1 bar can be used for detecting folding intermediates: By sampling the t_1 evolution in the reverse direction (Figure 1B-bottom), starting from the end of the low-pressure interval, after folding intermediates and folded proteins have developed, their signals will modulate the observed spectrum (Figure S3F,H). If the folding intermediate were resistant to high pressure, such a signal would resonate at the ^{1}H frequency of the folding intermediate during the ^{1}H detection period (F_2 dimension). However, as was observed previously in the classic interrupted folding experiments of Kiefhaber,[26, 58] intermediates are commonly less stable than the folded state and rapidly revert to the unfolded state once conditions are switched back to denaturing, i.e., high pressure. Therefore, the t_2-detected ^{1}H signal of the I state is found at the high-pressure unfolded ^{1}H frequency (Figure 2B and Figure 3B). For VA2-ubiquitin, we also find a minor fraction of I-state protein that switches to the native state prior to ^{1}H detection. This latter fraction gives rise to signals at the I-state ^{15}N frequency in the F_1 dimension, and to the native-state, high-pressure H^{N} frequency in the F_2 dimension (Figure S3H). The intensity ratio of the I-state peaks, correlated to the unfolded and folded H^{N} frequencies, corresponds to the ratio of the respective transition rates at high pressure $k_{I\rightarrow U} / k_{I\rightarrow F}$. The total amplitude of the folding intermediate signal, I, depends on the fraction of proteins that have switched to the intermediate state at time T after the drop to low pressure, but have not progressed to the folded state (Eq. 2). The integrated peak intensity of a U, I, or F resonance of the reverse-sampled time domain corresponds to the time domain point sampled at $t_1 = 0$, i.e., to the values $[U](T)$, $[I](T)$, and $[F](T)$, where T is the duration after the pressure drop at which the reverse sampling is started (Figure 1).

The decay profiles of the U-, I-, and F-state components with respect to t_1 are quite different from one another, with $[U](t_1)$ only being attenuated by true transverse relaxation, whereas $[I](t_1)$ and $[F](t_1)$ drop to zero at t_1=T, even in the absence of transverse relaxation, since no intermediate or folded magnetization is present immediately after the pressure drop. Details are presented in Supporting Information Figure S3. The different, non-exponential decay profiles for the $[I](t_1)$ and $[F](t_1)$ components result in non-Lorentzian line shapes after Fourier transformation, with the I and F state resonances being broader than those of the U fraction that remains unfolded during the low-pressure period (Figure S3). The differences in line shapes require that integrated peak intensities be measured to obtain accurate concentrations of the U-, I-, and F- states of ubiquitin. These intensities cannot easily be measured because of the crowded spectra obtained in our study. Nevertheless, the spectra

obtained by the reverse sampling method unambiguously reveal the ^{15}N and ^{13}C′ frequencies of the intermediate state.

Comparison of the forward sampled ^{15}N-^{1}H HSQC (Figure 2A) with the reverse sampled spectrum (Figure 2B) shows a multitude of new resonances in the latter. For example, the dashed red boxes outline correlations observed for residue S57. Each cross peak is marked by two superscripts, which refer to the state of the protein during t_1 evolution and during t_2 detection. For instance, the cross peak labeled S57^{IF} (top left in Figure 2B) corresponds to signal of the intermediate (I-state) ^{15}N frequency in the F_1 dimension, and the S57 ^{1}H frequency of the folded protein in the F_2 dimension. Note that the ^{1}H frequencies of the folded state at 2.5 kbar differ substantially from those at 1 bar but can easily be identified by recording a pressure jump ^{1}H-^{15}N 2D HSQC spectrum with preparation and ^{15}N evolution at 1 bar, and ^{1}H detection at 2.5 kbar (Figure S4). Figure 2A shows two intense resonances, S57^{UF} and S57^{UU}, from proteins that were unfolded at the end of the preparation period (marked “Prep.” in Figure 1), and either switched to the folded state during the low-pressure period (S57^{UF}) or remained unfolded (S57^{UU}). A very weak resonance, marked S57^{FF} (top left Figure 2A), corresponds to the small fraction (~6%) of proteins that remained folded at the end of the high-pressure preparation period. Because unfolding of the protein at high pressure is very slow, the corresponding S57^{FU} resonance has vanishing intensity. By contrast, the reverse sampled spectrum (Figure 2B) shows a strong S57^{FF} peak with just above it a very weak S57^{IF} peak from the small fraction of proteins that were in the intermediate state at the end of the low-pressure period but crossed the barrier to the folded state prior to ^{1}H detection. A considerably stronger S57^{IU} resonance, at the same ^{15}N F_1 frequency, is observed for I-state proteins that switched back to the unfolded state prior to ^{1}H detection. The slow unfolding rate at high pressure causes only a very small (~10%) fraction of proteins that had reached the folded state at the end of the low-pressure period to revert back to the unfolded state, giving rise to a very weak S57^{FU} peak (Figure 2B). A stronger S57^{UU} resonance corresponds to proteins that remained unfolded during the low-pressure interval.

Measurement of I-state ^{13}C′ chemical shifts.

Fully analogous to the forward and reverse sampled ^{15}N-^{1}H HSQC spectra, discussed above, the same forward and reverse sampling modes can be incorporated in the 2D HNCO pulse scheme (SI Figure S1C, D). The forward sampled HNCO spectrum then shows correlations between the U-state ^{13}C′ shift of residue *i* and the ^{1}H^{N} resonance of residue *i*+1 in both the unfolded and folded state. For example, the dashed vertical line in Figure 3A, at the ^{1}H^{N} frequency of residue L67 shows a correlation to T66-^{13}C′. At the same frequency in the reverse sampled spectrum (Figure 3B), the same T66^{UU} signal is observed, in addition to a correlation to the intermediate state, T66^{IU}, and a very weak resonance, T66^{FU} from proteins that were folded at the end of the low-pressure interval but subsequently unfold during the *ca.* 150-ms high-pressure period that separated ^{15}N evolution from ^{1}H detection. Analogous T66^{FF} and T66^{IF} signals are present in the full spectrum, outside the region shown in Figure 3. Although the signal-to-noise ratio of the HNCO spectra is nearly two-fold lower than for the HSQC spectra, recorded in a comparable amount of time, I-state ^{13}C′ resonances could be identified with confidence for 70 out of the potential 72 residues that are expected to give

rise to such signals. $^{13}C'$ signals of three residues preceding a Pro, the C-terminal residue G76 were missing, as well as M1 due to rapid exchange of the amide of Q2, while resonance overlap precluded assignment of I23 and D52 in the crowded region of the reverse sampled HNCO spectrum (Figure 3B; Figure S8).

Chemical shift characterization of the folding intermediate.

The ^{15}N chemical shifts of the folding intermediate measured from the folding-interrupted HSQC spectrum agree closely with values obtained previously from the pseudo-3D pressure-jump experiment (Figure 4), which measured the ensemble-averaged ^{15}N shift during the folding process by sampling a single time point in the indirect dimension (stroboscopic observation).[52] The I-state frequency was then extracted by means of a fitting procedure.[52] However, the stroboscopic measurement yielded relatively large uncertainties in the ensemble-averaged ^{15}N frequency of each residue, thereby adversely impacting the precision at which the frequency of the I-state component could be obtained. The current method yields highly precise peak positions but suffers from increased resonance overlap as the number of resonances in the reverse-sampled, folding-interrupted spectra is three-fold larger than that of the fully folded, or fully unfolded protein. Consequently, the set of residues for which unambiguous I-state ^{15}N frequencies could be determined is somewhat smaller (59 *vs.* 65 residues) than in the earlier work. With a root-mean-square difference (RMSD) of only 0.37 ppm (Figure 4B), agreement with the earlier measurement is very good, and results confirm that the I-state differs most from the F-state for the C-terminal strand, β5, and its preceding loop, strand β1, and the C-terminal residues of strand β3, with β5 being sandwiched between β1 and β3 in the natively folded state (Figure 5A,B).

^{15}N chemical shifts are exquisitely sensitive to a wide range of structural parameters, including H-bond strength, sidechain rotamer positioning, backbone torsion angles, and electrostatic effects from nearby charged groups,[59] complicating the interpretation of the ^{15}N chemical shift differences in structural terms. In contrast to ^{15}N, $^{13}C'$ chemical shifts correlate fairly well with protein secondary structure: $^{13}C'$ resonances in α-helical secondary structure are typically downfield shifted by 2–3 ppm from random coil, whereas upfield (negative) secondary shifts of 1–2 ppm are typically observed in β-sheet. Using the reverse sampled HNCO spectrum we obtained a set of 70 $^{13}C'$ I-state chemical shifts (Figure 5C–E). The chemical shifts of the I-state reveal important new information on the secondary structure of this transient structure. Particularly striking is the closeness of the I-state $^{13}C'$ shifts to those of the folded state for residues F4-T55. Substantial chemical shift differences between the folded and intermediate states are observed for residues S57-L73, which correspond to the C-terminal β5 strand, its preceding loop N60-S65, and the short 3_{10} helix preceding this loop. In addition, chemical shifts of residues Q2 and I3 in β1 differ considerably between I- and F-states. The secondary $^{13}C'$ shifts of Q2 and I3 in the I-state are *ca* −1.5 ppm, indicative of β-strand. Residues R72 and L73, which have close to random coil shifts in the native structure, show substantial negative and positive secondary shifts, respectively, in the I-state, indicative of well-defined structure for these residues. The chemical shift differences relative to the natively folded protein are mapped on a ribbon diagram of the folded structure (Figure 5E) and reveal more localized differences than previously seen from the ^{15}N chemical shift differences[52] (Figure 5B). Strands β3 and β1

pair with the C-terminal strand in the native structure, and it therefore appears likely that any significant difference in the N60-S65 loop, which contains two reverse turns in the native structure, could propagate into β5 and thereby β1. A structural analysis, including the collection of pressure-jump NOE data, currently in progress, will likely resolve the detailed structural differences between the intermediate and native states of the protein.

EXPERIMENTAL SECTION

Sample Preparation.

^{15}N- and ^{13}C-^{15}N-^{2}H-labeled VA2-ubiquitin was expressed and purified as described previously.[38] Importantly, a final HPLC step was found necessary to prevent proteolysis at high pressure, where the denatured state of the protein is highly susceptible to proteolytic cleavage. Samples were dissolved in 25 mM potassium phosphate buffer, pH 6.4, using 1% D_2O for a field frequency lock.

NMR spectroscopy.

All NMR experiments were recorded on a Bruker 600 MHz spectrometer equipped with cryogenic probehead with a z-axis pulsed field gradient accessory. A 2.8 mm ID zirconia sample cell, rated for static pressures of up to 3 kbar (Daedalus, Inc.) was used.[60] The hardware enabling rapid pressure switching, under control of the Bruker pulse program, has been described previously.[36] Both forward and reverse sampled pressure-jump HSQC spectra were recorded using a 210 μM uniformly ^{15}N-enriched sample of VA2-ubiquitin. The temperature was regulated at 25°C during the high-pressure period, but briefly drops by 3 °C during the low-pressure interval which had a total duration of *ca.* 70 ms. The depressurization transition evolves approximately linear in time during the period in which fluid flow through the transfer tube is turbulent, and transitions to a small exponential tail as the flow becomes laminar. Forward and reverse ^{15}N sampling was carried out for a 60 ms interval, which was initiated *ca.* 5 ms after the pressure drop to avoid encroaching on the tail end of the pressure drop. Inversely, the reverse sampling is initiated *ca.* 3 ms prior to the switch to high pressure to avoid encroaching on the high-pressure transition, which occasionally experiences ms timing jitter. A 150-ms delay separated the end of the low-pressure period from the reverse INEPT transfer of magnetization to ^{1}H for detection. This delay serves to let decay any mechanical vibrations in the system related to the pressure switches, which have their strongest impact on the high-γ ^{1}H signals. Spectra were recorded with 4 scans per free induction decay (FID), for a total of 120 complex t_1 increments per 2D spectrum. Using a recycle delay of 9 s, the total measurement time per spectrum was *ca.* 2.5 h. For the forward and reverse sampled 2D HNCO spectra, 100 complex t_1 increments were sampled, with 16 scans per FID, and a total measurement time of 8h per spectrum, using a 125 μM uniformly ^{13}C/^{15}N/^{2}H-labeled sample.

All the NMR data were processed and analyzed using NMRPipe[61] and NMRFAM-Sparky[62] software.

Supplementary Material

Refer to Web version on PubMed Central for supplementary material.

ACKNOWLEDGMENT

We thank J. Ying, Y. Shen, and J.L. Baber for technical support, and D.A. Torchia, T.R. Alderson, and G.M. Clore for useful discussions. This work was supported by the Intramural Research Program of the National Institute of Diabetes and Digestive and Kidney Diseases.

References

1. Dobson CM; Sali A; Karplus M, Protein folding: A perspective from theory and experiment. Angewandte Chemie-International Edition 1998, 37 (7), 868–893. [PubMed: 29711488]
2. Cellmer T; Henry ER; Hofrichter J; Eaton WA, Measuring internal friction of an ultrafast-folding protein. Proc. Natl. Acad. Sci. U. S. A 2008, 105 (47), 18320–18325. [PubMed: 19020085]
3. Chung HS; Louis JM; Eaton WA, Experimental determination of upper bound for transition path times in protein folding from single-molecule photon-by-photon trajectories. Proc. Natl. Acad. Sci. U. S. A 2009, 106 (29), 11837–11844. [PubMed: 19584244]
4. Chung HS; Gopich IV; McHale K; Cellmer T; Louis JM; Eaton WA, Extracting Rate Coefficients from Single-Molecule Photon Trajectories and FRET Efficiency Histograms for a Fast-Folding Protein. J. Phys. Chem. A 2011, 115 (16), 3642–3656. [PubMed: 20509636]
5. Chung HS; Eaton WA, Single-molecule fluorescence probes dynamics of barrier crossing. Nature 2013, 502 (7473), 685-+. [PubMed: 24153185]
6. Korzhnev DM; Kay LE, Probing invisible, low-populated states of protein molecules by relaxation dispersion NMR spectroscopy: An application to protein folding. Acc. Chem. Res 2008, 41 (3), 442–451. [PubMed: 18275162]
7. Korzhnev DM; Neudecker P; Zarrine-Afsar A; Davidson AR; Kay LE, Abp1p and fyn SH3 domains fold through similar low-populated intermediate states. Biochemistry 2006, 45 (34), 10175–10183. [PubMed: 16922492]
8. Bezsonova I; Korzhnev DM; Prosser RS; Forman-Kay JD; Kay LE, Hydration and packing along the folding pathway of SH3 domains by pressure-dependent NMR. Biochemistry 2006, 45 (15), 4711–4719. [PubMed: 16605239]
9. Matouschek A; Kellis JT; Serrano L; Fersht AR, Mapping the Transition-State and Pathway of Protein Folding by Protein Engineering. Nature 1989, 340 (6229), 122–126. [PubMed: 2739734]
10. Kim PS; Baldwin RL, Intermediates in the folding reactions of small proteins. Annu. Rev. Biochem 1990, 59, 631–660. [PubMed: 2197986]
11. Bai YW; Sosnick TR; Mayne L; Englander SW, Protein-Folding Intermediates - Native-State Hydrogen-Exchange. Science 1995, 269 (5221), 192–197. [PubMed: 7618079]
12. Schuler B; Lipman EA; Eaton WA, Probing the free-energy surface for protein folding with single-molecule fluorescence spectroscopy. Nature 2002, 419 (6908), 743–747. [PubMed: 12384704]
13. Vallee-Belisle A; Michnick SW, Visualizing transient protein-folding intermediates by tryptophan-scanning mutagenesis. Nat. Struct. Mol. Biol 2012, 19 (7), 731-+. [PubMed: 22683996]
14. Roder H, Structural characterization of protein folding intermediates by proton magnetic resonance and hydrogen exchange. Meth. Enzymol 1989, 176, 446–473. [PubMed: 2811697]
15. Englander SW; Mayne L, Protein Folding Studied Using Hydrogen-Exchange Labeling and 2-Dimensional Nmr. Annu. Rev. Biophys. Biomol. Struct 1992, 21, 243–265. [PubMed: 1525469]
16. Dyson HJ; Wright PE, How Does Your Protein Fold? Elucidating the Apomyoglobin Folding Pathway. Acc. Chem. Res 2017, 50 (1), 105–111. [PubMed: 28032989]
17. Eliezer D; Yao J; Dyson HJ; Wright PE, Structural and dynamic characterization of partially folded states of apomyoglobin and implications for protein folding. Nature Structural Biology 1998, 5 (2), 148–155. [PubMed: 9461081]
18. Krishna MMG; Maity H; Rumbley JN; Englander SW, Branching in the sequential folding pathway of cytochrome c. Protein Sci 2007, 16 (9), 1946–1956. [PubMed: 17660254]
19. Hollien J; Marqusee S, Comparison of the folding processes of T-thermophilus and E-coli ribonucleases H. J. Mol. Biol 2002, 316 (2), 327–340. [PubMed: 11851342]

20. Miranker A; Robinson CV; Radford SE; Aplin RT; Dobson CM, Detection of Transient Protein-Folding Populations by Mass-Spectrometry. Science 1993, 262 (5135), 896–900. [PubMed: 8235611]
21. Hu WB; Walters BT; Kan ZY; Mayne L; Rosen LE; Marqusee S; Englander SW, Stepwise protein folding at near amino acid resolution by hydrogen exchange and mass spectrometry. Proc. Natl. Acad. Sci. U. S. A 2013, 110 (19), 7684–7689. [PubMed: 23603271]
22. Hoeltzli SD; Frieden C, Stopped-flow NMR spectroscopy - Real-time unfolding studies of 6-F19-tryptophan-labeled E. Coli dihydrofolate reductase. Proc. Natl. Acad. Sci. U. S. A 1995, 92 (20), 9318–9322. [PubMed: 7568125]
23. Koide S; Dyson HJ; Wright PE, Characterization of a folding intermediate of apoplastocyanin trapped by proline isomerization. Biochemistry 1993, 32 (46), 12299–12310. [PubMed: 8241116]
24. Balbach J; Forge V; Vannuland NAJ; Winder SL; Hore PJ; Dobson CM, Following protein folding in real-time using NMR spectroscopy. Nature Structural Biology 1995, 2 (10), 865–870. [PubMed: 7552710]
25. Roche J; Dellarole M; Caro JA; Norberto DR; Garcia AE; Garcia-Moreno B; Roumestand C; Royer CA, Effect of Internal Cavities on Folding Rates and Routes Revealed by Real-Time Pressure-Jump NMR Spectroscopy. J. Am. Chem. Soc 2013, 135 (39), 14610–14618. [PubMed: 23987660]
26. Schlepckow K; Wirmer J; Bachmann A; Kiefhaber T; Schwalbe H, Conserved folding pathways of alpha-lactalbumin and lysozyme revealed by kinetic CD, fluorescence, NMR, and interrupted refolding experiments. J. Mol. Biol 2008, 378 (3), 686–698. [PubMed: 18377934]
27. Schanda P; Forge V; Brutscher B, Protein folding and unfolding studied at atomic resolution by fast two-dimensional NMR spectroscopy. Proc. Natl. Acad. Sci. U. S. A 2007, 104 (27), 11257–11262. [PubMed: 17592113]
28. Royer CA; Hinck AP; Loh SN; Prehoda KE; Peng XD; Jonas J; Markley JL, Effects of Amino-Acid Substitutions on the Pressure Denaturation of Staphylococcal Nuclease as Monitored by Fluorescence and Nuclear-Magnetic-Resonance Spectroscopy. Biochemistry 1993, 32 (19), 5222–5232. [PubMed: 8494899]
29. Yamaguchi T; Yamada H; Akasaka K, Thermodynamics of Unfolding of Ribonuclease-a under High-Pressure - a Study by Proton Nmr. J. Mol. Biol 1995, 250 (5), 689–694. [PubMed: 7623385]
30. Kitahara R; Hata K; Li H; Williamson MP; Akasaka K, Pressure-induced chemical shifts as probes for conformational fluctuations in proteins. Prog. Nucl. Magn. Reson. Spectrosc 2013, 71, 35–58. [PubMed: 23611314]
31. Urbauer JL; Ehrhardt MR; Bieber RJ; Flynn PF; Wand AJ, High-resolution triple-resonance NMR spectroscopy of a novel calmodulin peptide complex at kilobar pressures. J. Am. Chem. Soc 1996, 118 (45), 11329–11330.
32. Inoue K; Yamada H; Akasaka K; Hermann C; Kremer W; Maurer T; Doker R; Kalbitzer HR, Pressure-induced local unfolding of the Ras binding domain of RalGDS. Nature Structural Biology 2000, 7 (7), 547–550. [PubMed: 10876238]
33. Dumont C; Emilsson T; Gruebele M, Reaching the protein folding speed limit with large, sub-microsecond pressure jumps. Nat. Methods 2009, 6 (7), 515–U70. [PubMed: 19483692]
34. Kamatari YO; Yokoyama S; Tachibana H; Akasaka K, Pressure-jump NMR study of dissociation and association of amyloid protofibrils. J. Mol. Biol 2005, 349 (5), 916–921. [PubMed: 15907935]
35. Kremer W; Arnold M; Munte CE; Hartl R; Erlach MB; Koehler J; Meier A; Kalbitzer HR, Pulsed Pressure Perturbations, an Extra Dimension in NMR Spectroscopy of Proteins. J. Am. Chem. Soc 2011, 133 (34), 13646–13651. [PubMed: 21774550]
36. Charlier C; Alderson TR; Courtney JM; Ying J; Anfinrud P; Bax A, Study of protein folding under native conditions by rapidly switching the hydrostatic pressure inside an NMR sample cell. Proc. Natl. Acad. Sci. USA 2018, 115, E4169–E4178. [PubMed: 29666248]
37. Harper SM; Neil LC; Day IJ; Hore PJ; Gardner KH, Conformational changes in a photosensory LOV domain monitored by time-resolved NMR spectroscopy. J. Am. Chem. Soc 2004, 126 (11), 3390–3391. [PubMed: 15025443]

38. Alderson TR; Charlier C; Torchia DA; Anfinrud P; Bax A, Monitoring Hydrogen Exchange During Protein Folding by Fast Pressure Jump NMR Spectroscopy. J. Am. Chem. Soc 2017, 139 (32), 11036–11039. [PubMed: 28766333]
39. Krantz BA; Sosnick TR, Distinguishing between two-state and three-state models for ubiquitin folding. Biochemistry 2000, 39 (38), 11696–11701. [PubMed: 10995237]
40. Khorasanizadeh S; Peters ID; Butt TR; Roder H, Folding and Stability of a Tryptophan-Containing Mutant of Ubiquitin. Biochemistry 1993, 32 (27), 7054–7063. [PubMed: 8392867]
41. Larios E; Li JS; Schulten K; Kihara H; Gruebele M, Multiple probes reveal a native-like intermediate during low-temperature refolding of ubiquitin. J. Mol. Biol 2004, 340 (1), 115–125. [PubMed: 15184026]
42. Herberhold H; Winter R, Temperature- and pressure-induced unfolding and refolding of ubiquitin: A static and kinetic Fourier transform infrared spectroscopy study. Biochemistry 2002, 41 (7), 2396–2401. [PubMed: 11841233]
43. Sosnick TR; Dothager RS; Krantz BA, Differences in the folding transition state of ubiquitin indicated by phi and psi analyses. Proc. Natl. Acad. Sci. U. S. A 2004, 101 (50), 17377–17382. [PubMed: 15576508]
44. Rea AM; Simpson ER; Meldrum JK; Williams HEL; Searle MS, Aromatic Residues Engineered into the beta-Turn Nucleation Site of Ubiquitin Lead to a Complex Folding Landscape, Non-Native Side-Chain Interactions, and Kinetic Traps. Biochemistry 2008, 47 (48), 12910–12922. [PubMed: 18991391]
45. Vallee-Belisle A; Michnick SW, Multiple tryptophan probes reveal that ubiquitin folds via a late misfolded intermediate. J. Mol. Biol 2007, 374 (3), 791–805. [PubMed: 17949746]
46. Piana S; Lindorff-Larsen K; Shaw DE, Atomic-level description of ubiquitin folding. Proc. Natl. Acad. Sci. U. S. A 2013, 110 (15), 5915–5920. [PubMed: 23503848]
47. Vajpai N; Nisius L; Wiktor M; Grzesiek S, High-pressure NMR reveals close similarity between cold and alcohol protein denaturation in ubiquitin. Proc. Natl. Acad. Sci. U. S. A 2013, 110 (5), E368–E376. [PubMed: 23284170]
48. Reddy G; Thirumalai D, Collapse Precedes Folding in Denaturant-Dependent Assembly of Ubiquitin. J. Phys. Chem. B 2017, 121 (5), 995–1009. [PubMed: 28076957]
49. Reddy G; Thirumalai D, Dissecting Ubiquitin Folding Using the Self-Organized Polymer Model. J. Phys. Chem. B 2015, 119 (34), 11358–11370. [PubMed: 26131594]
50. Khorasanizadeh S; Peters ID; Roder H, Evidence for a three-state model of protein folding from kinetic analysis of ubiquitin variants with altered core residues. Nature Structural Biology 1996, 3 (2), 193–205. [PubMed: 8564547]
51. Went HM; Benitez-Cardoza CG; Jackson SE, Is an intermediate state populated on the folding pathway of ubiquitin? FEBS Lett 2004, 567 (2–3), 333–338. [PubMed: 15178347]
52. Charlier C; Courtney JM; Alderson TR; Anfinrud P; Bax A, Monitoring N-15 Chemical Shifts During Protein Folding by Pressure-Jump NMR. J. Am. Chem. Soc 2018, 140 (26), 8096–8099. [PubMed: 29923716]
53. Erlach MB; Koehler J; Crusca E; Kremer W; Munte CE; Kalbitzer HR, Pressure dependence of backbone chemical shifts in the model peptides Ac-Gly-Gly-Xxx-Ala-NH2. J. Biomol. NMR 2016, 65 (2), 65–77. [PubMed: 27335085]
54. Bax A; Pochapsky SS, Optimized Recording of Heteronuclear Multidimensional Nmr- Spectra Using Pulsed Field Gradients. J. Magn. Reson 1992, 99 (3), 638–643.
55. Keeler J; Clowes RT; Davis AL; Laue ED, Pulsed-Field Gradients - Theory and Practice. Meth. Enzymol 1994, 239, 145–207. [PubMed: 7830583]
56. Bax A; Ikura M; Kay LE; Torchia DA; Tschudin R, Comparison of different modes of two-dimensional reverse-correlation NMR for the study of proteins. J. Magn. Reson 1990, 86, 304–318.
57. Ikura M; Kay LE; Bax A, A novel approach for sequential assignment of 1H, 13C, and 15N spectra of larger proteins: heteronuclear triple-resonance three-dimensional NMR spectroscopy. application to calmodulin. Biochemistry 1990, 29 (19), 4659–4667. [PubMed: 2372549]
58. Kiefhaber T, Kinetic traps in lysozyme folding. Proc. Natl. Acad. Sci. U. S. A 1995, 92 (20), 9029–9033. [PubMed: 7568066]

59. de Dios AC; Pearson JG; Oldfield E, Secondary and tertiary structural effects on protein NMR chemical shifts - an ab initio approach. Science 1993, 260 (5113), 1491–1496. [PubMed: 8502992]

60. Peterson RW; Wand AJ, Self-contained high-pressure cell, apparatus, and procedure for the preparation of encapsulated proteins dissolved in low viscosity fluids for nuclear magnetic resonance spectroscopy. Rev. Sci. Instrum 2005, 76 (9).

61. Delaglio F; Grzesiek S; Vuister GW; Zhu G; Pfeifer J; Bax A, NMRpipe - a multidimensional spectral processing system based on Unix pipes. J. Biomol. NMR 1995, 6 (3), 277–293. [PubMed: 8520220]

62. Lee W; Tonelli M; Markley JL, NMRFAM-SPARKY: enhanced software for biomolecular NMR spectroscopy. Bioinformatics 2015, 31 (8), 1325–1327. [PubMed: 25505092]

63. Nielsen JT; Mulder FAA, POTENCI: prediction of temperature, neighbor and pH-corrected chemical shifts for intrinsically disordered proteins. J. Biomol. NMR 2018, 70, 141–175. [PubMed: 29399725]

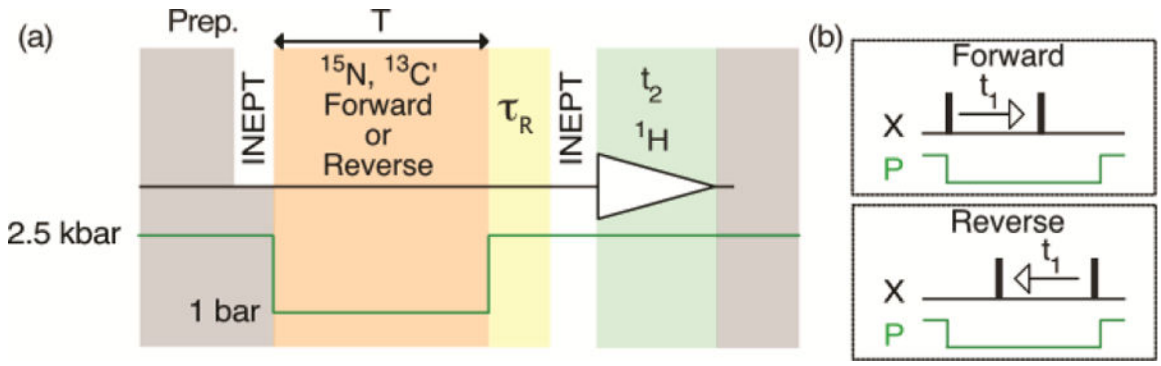

Figure 1.

Simplified schematic of the forward and reverse detected pressure-jump 2D ^{1}H-^{15}N HSQC and ^{1}H-^{13}C′ HNCO experiments. In both schemes, the spin system is prepared (Prep.) by a long (*ca.* 10 s) high pressure protein denaturation interval, which is terminated by a refocused INEPT transfer to $^{15}N_z$ magnetization (HSQC) or to antiphase $^{13}C'_z{}^{15}N_z$ magnetization (HNCO). During the subsequent low pressure period (total duration T, *ca.* 70 ms) the ^{15}N (HSQC) or ^{13}C′ (HNCO) frequency is encoded either in the regular, forward manner (B, top), or in the reverse manner (B, bottom), where the second ^{15}N (HSQC) or ^{13}C′ (HNCO) pulse is always applied just prior to the jump back to high pressure, and the first pulse is moved stepwise to the left. Protein folding takes place during the low-pressure interval but is interrupted by the jump back to high pressure, prior to signal detection. A vibration decay delay (yellow, ~150 ms), where magnetization is stored along the *z* axis, precedes transfer of magnetization to ^{1}H for detection during t_2. Full details of the pulse sequence are provided in SI Figure S1.

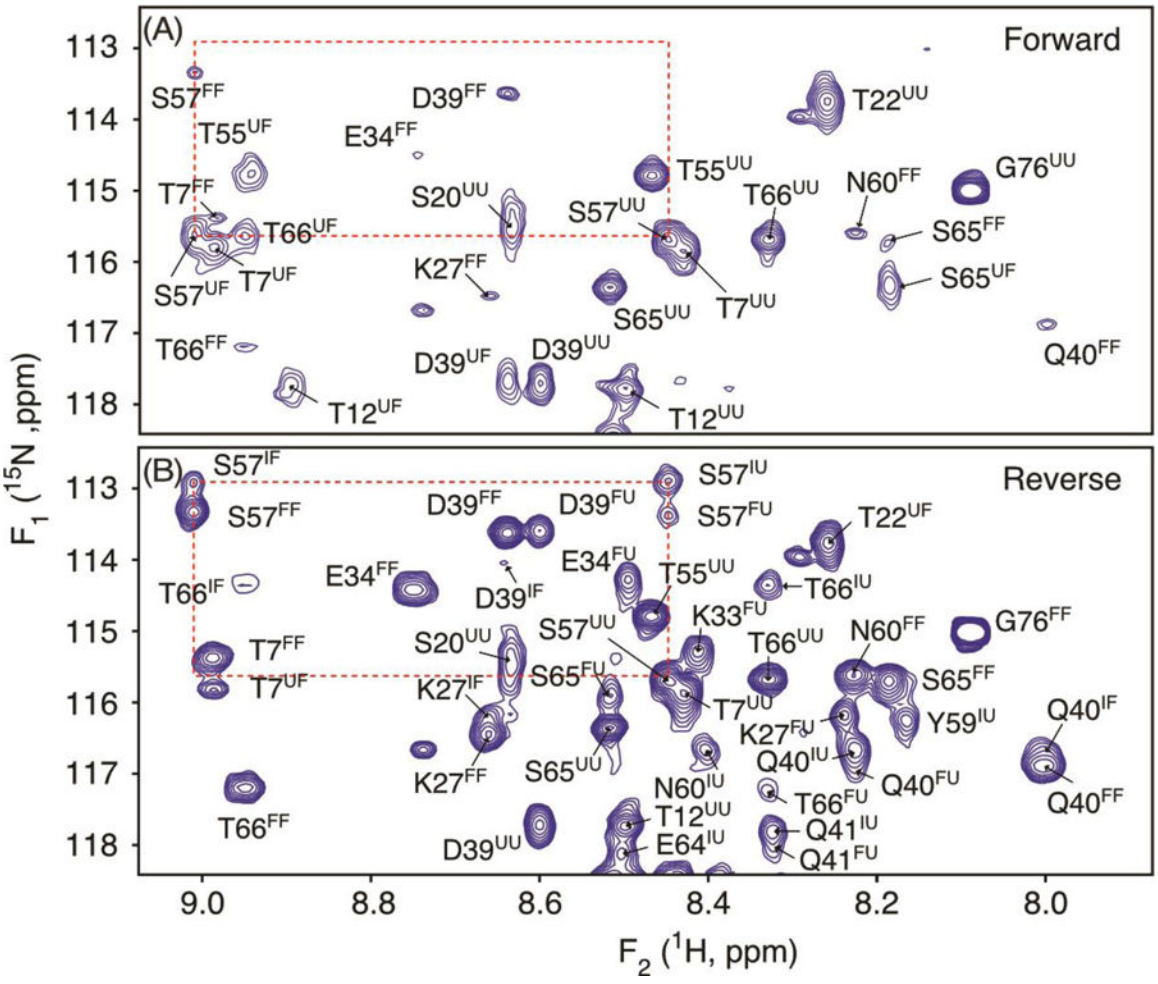

Figure 2.

Small regions of the (A) forward and (B) reverse sampled 2D ^{1}H-^{15}N HSQC spectra of a sample containing 210 mM ^{15}N ubiquitin, pH 6.4. Full spectra are shown in Figures S5 and S6. Spectra are recorded at 600 MHz ^{1}H frequency, using a cryogenic probehead equipped with a z-axis pulsed field gradient accessory. The temperature was regulated at 25 °C but drops by 3 °C due to adiabatic expansion during the brief low-pressure period. The forward recorded spectrum (A) primarily shows F_1 dimension correlations for species present at the start of the low-pressure period, i.e. unfolded protein. These signals are correlated in the F_2 dimension with unfolded ^{1}H frequencies at 2.5 kbar for proteins that did not cross the folding barrier during the low-pressure period, or to folded ^{1}H frequencies at 2.5 kbar for proteins that crossed the folding barrier. The reverse sampled spectrum (B) shows in the F_1 dimension the ^{15}N frequencies of all species present at the end of the low-pressure period, i.e., unfolded, intermediate, and folded, correlated with their respective ^{1}H frequency at high pressure. Correlations are labeled by residue number, with the first superscript referring to the ^{15}N chemical shift of the unfolded (U), Intermediate (I) or Folded (F) state at the end of the low-pressure interval, and the second superscript denoting the state of the protein during detection. No I-state ^{1}H signals are observed because the majority of I-state proteins revert to U prior to detection; a *ca.* 2-fold smaller fraction crosses the barrier to the folded state,

yielding resonances superscripted IF. The pattern of correlations for S57 is marked by red dashed rectangles.

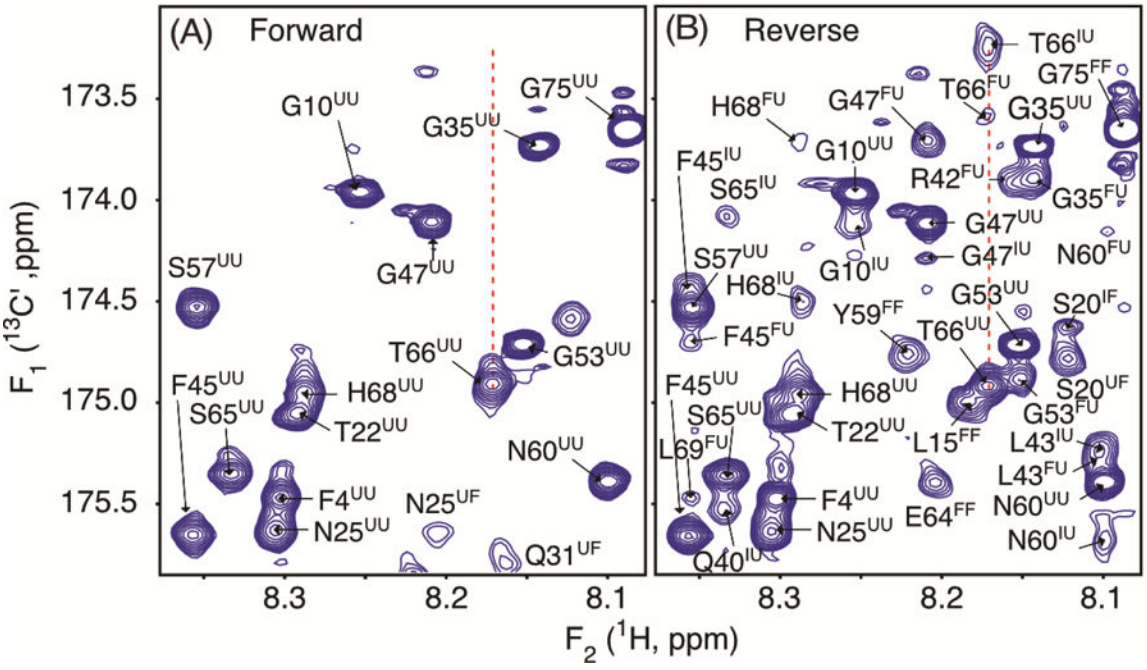

Figure 3.

Small regions of the 600 MHz (A) forward and (B) reverse sampled 2D ^{1}H-^{13}C′ HNCO spectra of a sample containing 125 μM ^{15}N/^{13}C′/^{2}H-VA2-ubiquitin, pH 6.4, 25 °C. Full spectra are shown in Figures S7 and S8. Fully analogous to the spectra of Figure 2, the forward spectrum (A) primarily shows F_1 dimension correlations for unfolded protein, correlated to 2.5 kbar ^{1}H F_2 frequencies of either folded or unfolded protein. Analogously, the reverse sampled spectrum (B) shows in the F_1 dimension the 1-bar ^{13}C′ frequencies of U, I, and F species, correlated with 2.5 kbar ^{1}H frequency of the amide of the next residue. Each peak number indicates the residue that is ^{13}C′ labeled, with the first superscript referring to the state of the protein during ^{13}C′ evolution at 1 bar, and the second superscript denoting the state during ^{1}H detection at 2.5 kbar.

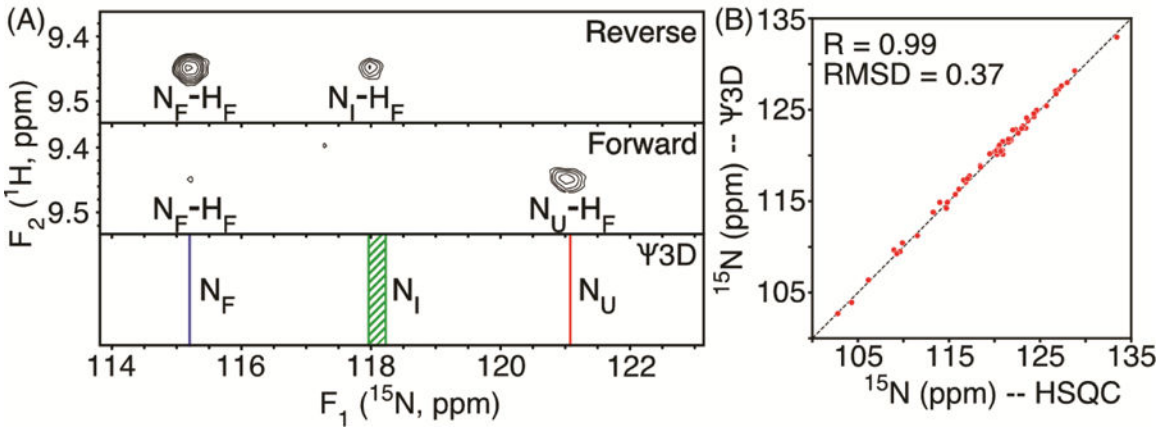

Figure 4.

Comparison of spectral data of the E64 amide of VA2-ubiquitin, recorded with the pressure-jump 2D ^{1}H-^{15}N HSQC experiment of Figure 1, and ^{15}N chemical shifts previously derived from stroboscopic observation of ^{15}N shifts in a pseudo-3D (Ψ3D) measurement.[52] (A) ^{15}N F_1 strips taken at the E64 F_2 $^1H^N$ frequency of folded ubiquitin at 2.5 kbar, with the bottom strip showing the results of previous fitting of the Ψ3D data of this residue. (B) Correlation plot of the ^{15}N I-shifts extracted from the Ψ3D spectrum (*y*-axis) with those of the reverse-sampled pressure-jump HSQC spectrum (*x*-axis). The Pearson correlation coefficient equals 0.99, with an RMSD of 0.37 ppm.

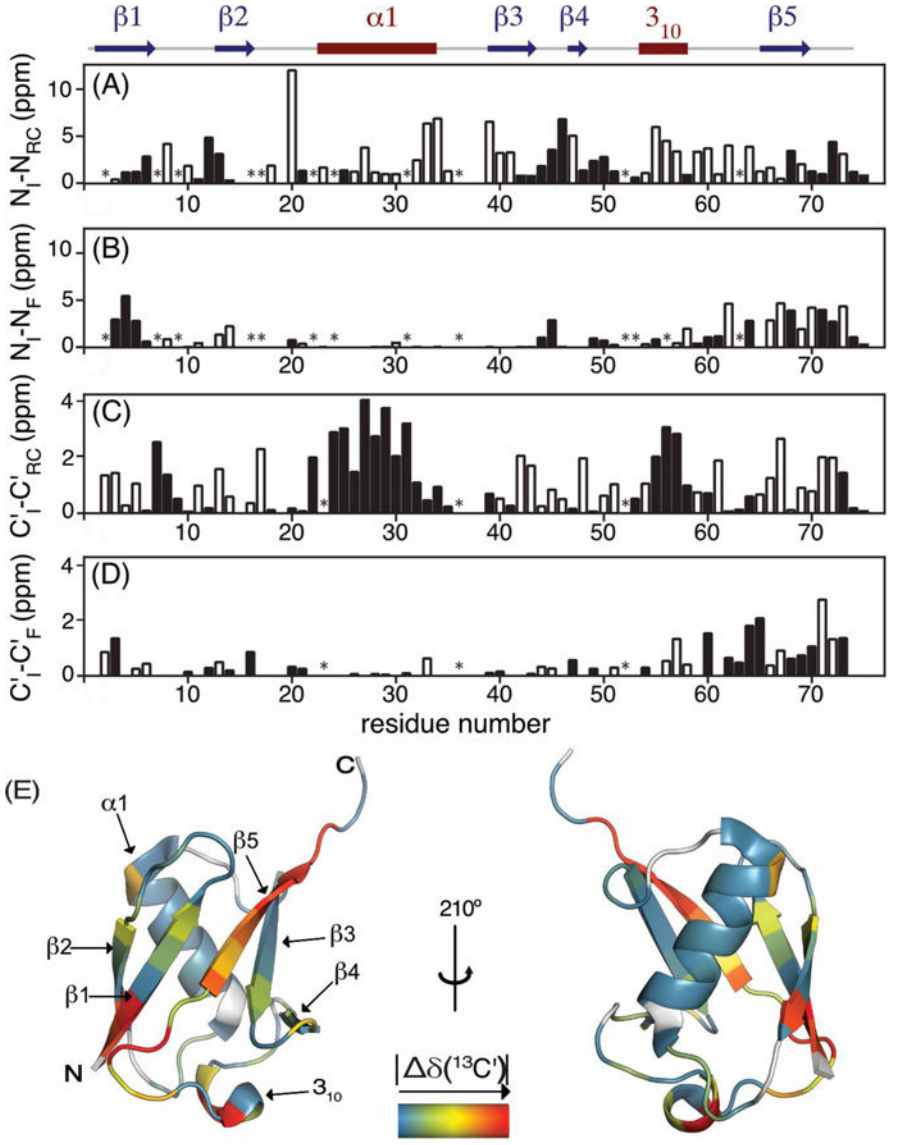

Figure 5.

Comparison of 1-bar ^{15}N and $^{13}C'$ chemical shifts of the VA2-ubiquitin folding intermediate with those of the folded state (δ^F) and with random coil values (δ^{RC}) obtained with the program POTENCI.[63] Filled and open bars correspond to positive and negative values, respectively. (A) $\delta^I(^{15}N) - \delta^F(^{15}N)$; (B) $\delta^I(^{15}N) - \delta^{RC}(^{15}N)$; (C) $\delta^I(^{13}C') - \delta^F(^{13}C')$; (D) $\delta^I(^{13}C') - \delta^{RC}(^{13}C')$; (E) $|\Delta\delta(^{13}C')| = |\delta^I(^{13}C') - \delta^F(^{13}C')|$ color coded on a backbone ribbon structure of the native state of ubiquitin (PDB entry 2MJB). Residues for which $|\Delta\delta(^{13}C')|$ could not be determined are shown in grey.